RESEARCH ARTICLE

ADVANCED OPTICAL MATERIALS
www.advopticalmat.de

Rapidly Grown Hexagonal Organic Microtubes Using Ionic Liquids for an Enhanced Optical Waveguide Effect

Do Wan Kim, Jongchan Kim, Yongmin Baek, Kyusung Choi, Jiyoun Kim, Sung Ho Yoo, Jinwoo Song, Jihoon Choi, Heesoh Noh, Kyusang Lee, Jae-Won Jang,* and Dong Hyuk Park**

An optical waveguide that transmits the electromagnetic waves is a critical component for various optoelectrical applications including integrated optical circuits and optical communications. Among many, the 1D tubular optical waveguide structure enables efficient distant energy transfer via mode selection within the optical microcavity. However, its application is limited due to the complicated fabrication process. Herein, hexagonal tris(8-hydroxyquinoline) aluminum (Alq_3) microtubes with an average longitudinal length of ≈15 µm are self-assembled within few minutes by utilizing 1-butyl-3-methylimidazolium tetrafluoroborate ($BMIMBF_4$) ionic liquids. The swift fabrication is enabled by the high electron affinity of $BMIMBF_4$ that forms hexagonal microrods. Also, BMIMBF4 ionic liquid etches the central region of micorods during its growth, forming microtubes with a wall thickness of ≈650 nm. The fabricated Alq_3 microtubes show significantly improved waveguide characteristics with reduced optical loss coefficient (0.054 μm^{-1}) compared to that of microrods (0.271 μm^{-1}). The demonstrated method to fabricate Alq_3 microtubes with ionic liquid is an efficient approach to utilize organic microstructures as an optoelectrical components for advanced optical communications.

1. Introduction

Developing facile methods for fabricating low-optical-loss waveguide structures in nano- and micro-scale using top-down approach have been a challenge to be employed for optical communication applications.[1] As an alternative, organic semiconductor molecules based nano- to micro-scale 1D structures can be effectively built by bottom-up approach using self-assembling process to propagate light through it.[2] Moreover, cavity-like 1D organic microstructures can easily generate Frenkel excitons that are strongly coupled with photons to form exciton polaritons with excellent propagation characteristics.[1d,3] Fabrication of 1D organic microstructures are usually achieved by template-based growth[4] and physical vapor deposition (PVD)[5]; however, it often suffers from poor crystallinity[4d,e] and is sensitive to the experimental conditions.[5c,6] There are also other fabrication methods such as electrospinning[7] and vaporization-condensation-recrystallization process[8] but they require tricky exerimental conditions to achieve 1D tubular strucutre with high crystallinity. Alternatively, solution-based self-assembly techniques of the π-conjugated organic molecules offer facile procedures for the fabrication of well-defined 1D organic nano/micro-structures[9] with exquisite crystallinity. Such high

D. W. Kim, J.-W. Jang
Division of Physics and Semiconductor Science
Dongguk University
Seoul 04620, Republic of Korea
E-mail: jwjang@dgu.ac.kr

J. Kim, K. Choi
Department of Integrated Display Engineering
Yonsei University
Seoul 03722, Republic of Korea

Y. Baek, K. Lee
Department of Electrical and Computer Engineering
University of Virginia
Charlottesville, VA 22904, USA
E-mail: kyusang@virginia.edu

J. Kim, S. H. Yoo, J. Song, D. H. Park
Department of Chemical Engineering
Inha University
Incheon 22212, Republic of Korea
E-mail: donghyuk@inha.ac.kr

J. Kim, S. H. Yoo, J. Song, D. H. Park
Program in Biomedical Science and Engineering
Inha University
Incheon 22212, Republic of Korea

J. Choi, H. Noh
Department of Nano and Electronic Physics
Kookmin University
Seoul 02707, Republic of Korea

K. Lee
Department of Material Science and Engineering
University of Virginia
Charlottesville, VA 22904, USA

The ORCID identification number(s) for the author(s) of this article can be found under https://doi.org/10.1002/adom.202303077

DOI: 10.1002/adom.202303077

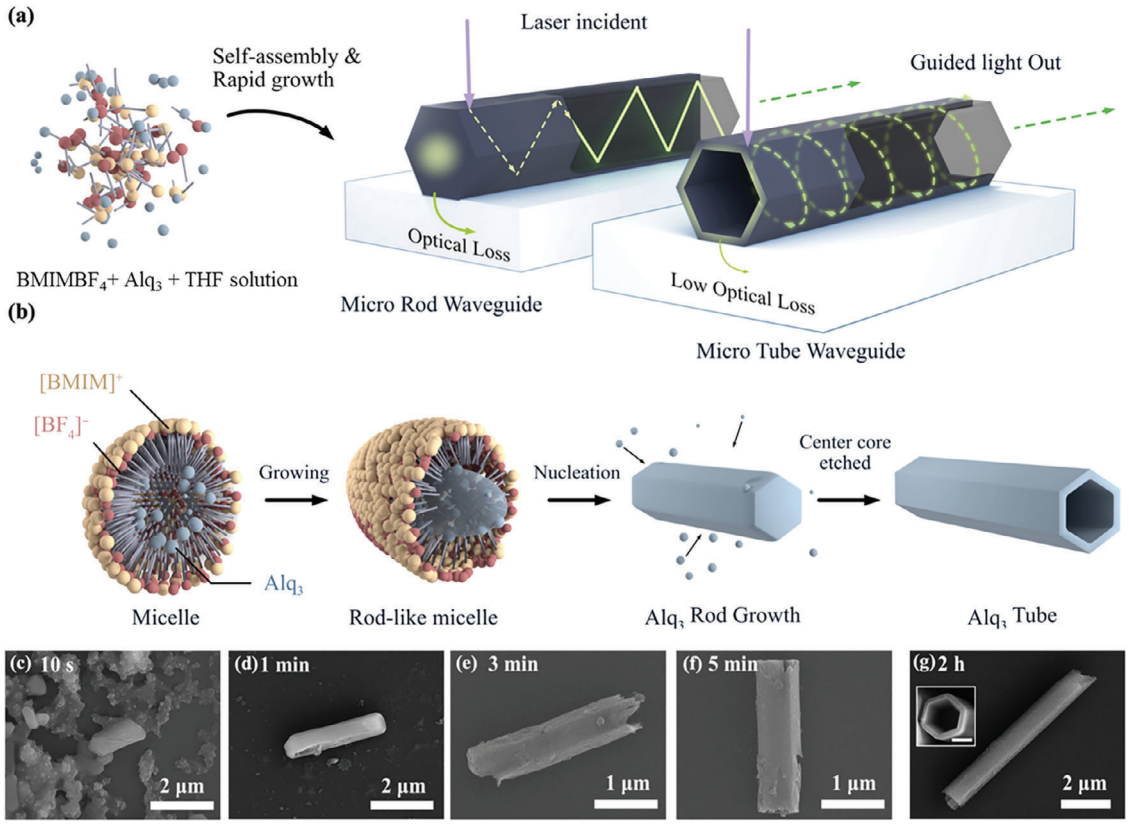

Figure 1. a) Schematic illustration of Alq_3 microstructures synthesis method and their waveguiding characteristics. b) Scheme for a facile self-assembly sequence of Alq_3 microtubes in $BMIMBF_4$ solution. (c-g) SEM images of Alq_3 microstructures after mixing in the $BMIMBF_4$ solution for c) 10 s, d) 1 min, e) 3 min, f) 5 min, and g) 2 h. Inset: a zoomed SEM image in the radial direction of an Alq_3 microtube (Scale bar: 500 nm).

crystallinity of the π-conjugated organic molecules is advantageous in generating more excitons and propagating light with minimal losses, allowing their applications for functional optical devices.[2b,10] As a result, various applications of organic nano/microstructures to lasers,[4e,11] waveguides,[9b,11a,b,12] solar cells,[13] and sensors[5d,14] have been demonstrated. Among many, tubular nanostructures fabricated with organic small molecules show exceptional optical waveguiding performances since they are mostly surrounded by low-refractive-index air media, which suppresses the guided signal leakage toward the substrate[5c,15] and photons are effectively confined in the thin walls.[1d,16] However, fabricating tubular nanostructures with organic molecules via solution self-assembly techniques remains a challenge[17] since it requires long fabrication time up to several hours.[5c,18]

Herein, we demonstrate a rapid growth of tris(8-hydroxyquinoline) aluminum (Alq_3) microrods and microtubes by introducing 1-butyl-3-methylimidazolium tetrafluoroborate ($BMIMBF_4$) ionic liquids during the solution self-assembly process. The relatively high E_T^N value (0.673) of $BMIMBF_4$ ionic liquid accelerates the aggregation of the Alq_3 molecules enabling the growth of Alq_3 microrods in few minutes.[19] Moreover, $BMIMBF_4$ ionic liquid etch out the Alq_3 microrods from the cores that forms Alq_3 microtubes from microrods. As a result, the optical loss was suppressed in an order of magnitude with the microtube. Furthermore, the ionic liquid used in this work is environmentally friendly with high chemical and thermal stability compared to other commonly used organic solvents[20] for synthesis[4d] and liquid-liquid extraction.[21] Hence, the method shown enables an efficient and environmentally friendly fabrication of nano- and micro-scale tubes for their widespread applications in optoelectronics.

2. Results and Discussion

We have developed a self-assembly and rapid growth process to fabricate Alq_3 microrod and microtube waveguides. The fabricated microstructures confine and guide incident light through the interior of the microrods and along the thin tubular walls of the microtubes with low optical losses (**Figure 1a**). Figure 1b shows a schematic illustration of the fabrication procedure of the micro- and nano-tubes. First, Alq_3 powder dissolved in tetrahydrofuran (THF) is mixed with $BMIMBF_4$ solution by stirring (See *Methods* for more details). The solution is then dropcasted on a cover glass and dried. During the stirring process, Alq_3 microstructures are synthesized through the following processes; i) $BMIMBF_4$ ions accelerate the aggregation of Alq_3 molecules to form small micelles, ii) Small micelles are grown into rod-like structures, iii) nucleation of Alq_3 triggers longitudinal growth of microrods with an average length of 1–2 μm, iv) the core of the microrods are etched out during the longitudinal growth of the Alq_3, resulting in tens-of-micrometers-long Alq_3 microtubes.

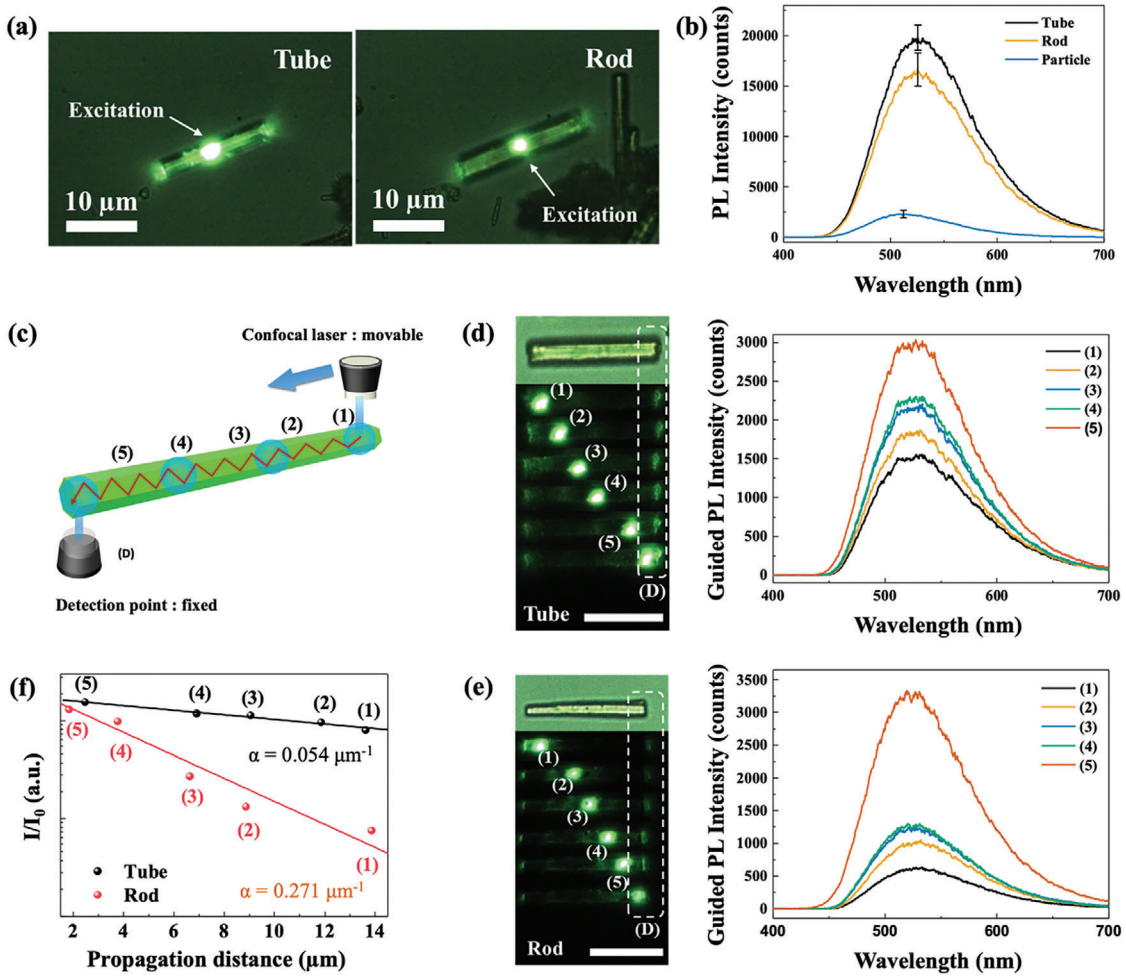

Figure 2. a) CCD images of an Alq_3 microtube (top) and an Alq_3 microrod (bottom) with 405 nm laser excitation at the center of the samples. b) PL spectra of the Alq_3 microtube (Tube), microrod (Rod), and particle (Particle). c) Schematic illustration of the experimental setup for measurement of light propagation characteristics. (d,e) CCD images of d) Alq_3 microtube (Tube) and e) microrod (Rod) with five different excitation points (1~5, scale bar: 10 μm). The top images obtained without excitation light. (Right) The corresponding PL spectra measured at the detection point (D) of (d,e). f) Logarithmic plots of the relative peak intensities of the Alq_3 microtube (Tube) and microrod (Rod) as functions of propagation distance; the black and red lines represent an exponential decay fit of the samples.

The core of the Alq_3 seems to have highest attachment energy or surface free energy having strong attraction for the organic molecules of THF or $BMIMBF_4$, and thus preferentially etching out the core first.[22] Eventually, the walls of the Alq_3 start to break down when the mixing time exceeds 3 h (Figure S1, Supporting Information).

SEM images of Alq_3 microrods with the processing time of 10 s; 1, 3, and 5 min; and 2 h are shown in Figure 1c–g. Alq_3 molecules aggregate within 10 s when the Alq_3/THF solution is mixed with $BMIMBF_4$ due to the $BMIMBF_4$ cations and anions that forms small rod-like micelles (Figure 1c).[19c] After 1 min of stirring, microrods with a length of ≈3 μm are observed, which still grows in the longitudinal direction by absorbing nearby Alq_3 molecules (Figure 1d). As the mixing time increases to 3–5 min, Alq_3 keeps on growing to the longitudinal direction of the hexagonal microrods. The core of the rods is decomposed during the growth (Figure 1e,f). Within 2 h, ≈15 μm long Alq_3 microtubes with diameters ranging from 1 to 2 μm are grown (Figure 1g). SEM images of Alq_3 microstructures and intermediate states of growth depending on mixing times are provided in Supporting Information (Figure S2, Supporting Information). According to the characterization of Alq_3 microstructures depending on the processing time, the length of the Alq_3 microstructures increases as the reaction time increases while the diameter of the Alq_3 microstructures remains nearly identical.

Color charge-coupled device (CCD) images and photoluminescence (PL) spectra are obtained in **Figure 2** to investigate the optical properties of the Alq_3 microstructures. Figure 2a shows the CCD images of an Alq_3 microtube (left) and a microrod (right) with a 405 nm laser excitation at the center of the samples. In addition to the PL at the excitation location, guided light at the ends of the microtube and microrod is observed. The guided light at the edge of the structure is observed to be stronger in the Alq_3 microtube compared to the microrod, confirming an improved optical waveguide performance of the microtube. For a quantitative comparison of the emission characteristics, the PL spectra of

the Alq_3 microrod, microtube, and Alq_3 particle (irregular-shaped micelles in Figure 1c) are obtained (Figure 2b). The Alq_3 particle exhibits the smallest PL intensity with the emission peak centered at 510 nm. Meanwhile, a redshift of PL peak to 525 nm is observed for both microtube and microrod due to the formation of meridional Alq_3 structure.[23] In addition, the PL intensities are increased by eight and six times for the microtube and microrod, respectively, compared to the Alq_3 particle due to the improved crystallinity of the Alq_3 microstructures during the solution self-assembly process.[24] The improved crystallinity of the Alq_3 microstructures is also verified by detection of α-stacking peaks in their XRD spectra,[24,25] while no XRD peak is observed in the Alq_3 particle (Figure S3, Supporting Information). The additional increment of PL intensity of the microtube compared to the microrod is due to the optical confinement of photons in the thin wall.[26]

The propagation loss is measured to characterize the optical waveguide properties of the Alq_3 microstructures. As illustrated in Figure 2c, the PL intensities of the guided light are detected at the ends of the microtube and microrod (denoted by D) with the excitation laser (405 nm) positioned at five different points with spacing of ≈2 μm (denoted with 1 to 5 in Figure 2d,e). The CCD images of Alq_3 microrod (top) and microtube (bottom) with the guided PL spectra (right) are displayed in Figure 2d,e, respectively. As the excitation laser moves closer to the detection point, the waveguided PL intensities increase in both the Alq_3 microtube and microrod. As shown in the PL spectra, the PL intensity of the microrod decreases more significantly (approximately two times) than that of the microtube when the laser is moved from position (5) to (1-4). To compare the optical loss through microrod and microtube, the relative intensities of the waveguided PL peaks through the microtube and microrod are plotted as functions of propagation distance (Figure 2f). The optical loss coefficients are derived by the following equation,[3c]

$$\frac{I}{I_0} = e^{-\alpha x} \tag{1}$$

where I and I_0 are the intensity of the guided and unguided light, respectively. x is the propagation distance from the excitation position to the detection point and α is the optical loss coefficient. The optical loss coefficient of the microtube obtained from the fitting is shown to be 0.054 μm^{-1}, approximately five times lower than that of the microrod (0.271 μm^{-1}). The average loss coefficients of the Alq_3 microtubes and microrods are obtained from five samples to be 0.086 and 0.236 μm^{-1}, respectively (Figure S4, Supporting Information). The superior waveguide performance of the Alq_3 microtube is possibly attributed to the suppressed guided signal leakage to the substrate in the microtube.[15a] The optical loss coefficient of the Alq_3 microtube is much lower compared to the previously reported result in bio-hybrid Alq_3 microrods (0.159 μm^{-1}).[14] Meanwhile, there are other comparable reports of 1D organic waveguides with lower optical loss coefficients, especially in hybrid or doped materials.[3c,5c] Similar manipulation on Alq_3 microstructures can be introduced to enhance the propagation properties.

The optical loss coefficients of the Alq_3 microtube and microrod are calculated by the finite element method (FEM, COMSOL) to theoretically compare the optical loss through the microtube and microrod. First, eigenmodes at 520 nm of both Alq_3 microstructures which is the peak wavelength of the PL spectra, are derived in the radial direction (**Figure 3a**). Due to the absorption of Alq_3, light decays faster in the center of microrod. Thus, the eigenmode with the electric field (E-field) is more strongly distributed at the surface of the tube structure compared to that of rod structure. To confirm the propagation of the E-field along the longitudinal axis, the Alq_3 microstructures are simulated to be excited with the corresponding wavelength (520 nm) at the left end of the 1D microstructure with 650 nm width (the red arrows in Figure 3b). In case of microrod, the E-field is the strongest in the center of the rod and propagates through the core. On the other hand, in case of microtube, the E-field is concentrated in and propagates through the thin wall of the tube. Furthermore, a rapid decay of the E-field occurs in the microrod along the longitudinal direction, while the decline is suppressed in the microtube. To theoretically calculate the optical loss coefficients of the microstructures, logarithmic plots of normalized intensities of the inletting E-field are displayed as functions of propagation distance (Figure 3c). The plots are fit with Equation 1, where the fitted curves are plotted in solid lines. The optical loss coefficients are calculated as 0.028 and 0.152 μm^{-1} for the microtube and microrod, respectively.

The theoretical optical loss coefficients of the Alq_3 microstructures are lower than those of the experimental values (0.054 and 0.271 μm^{-1}, respectively), due to the absence of the substrate in the simulations. Owing to the omitted E-field leakage to the substrate in the simulation, a lower optical loss coefficient from the theoretical calculations is observed. Though the silicon substrate is excluded in the theoretical simulations, the optical loss coefficient of the microtube is approximately five times lower than that of the microrod (similar to the experimental observations), demonstrating a superior waveguiding performance (lower optical loss coefficient) in the microtube compared to the microrod.

The fabricated Alq_3 microstructures were incorporated with trimethine cyanine dye (Cy3) during self-assembly, as shown in **Figure 4a**. Cy3 is a fluorescent chemosenor used for labeling bio/chemical materials such as nucleic acids.[14,27] Figure 4b shows the CCD images of the Cy3 conjugated to the entire tube (Cy3-tube, top) and the entire rod (Cy3-rod, bottom) with the excitation laser focused at the center of each respective structure. Aside from the Alq_3 emission (λ = 500 nm), a PL of Cy3 (λ = 590 nm) occurs at the edge of the waveguide, due to the Förster resonance energy transfer (FRET) between Alq_3 and Cy3. The Cy3 PL is notably stronger in the microtube than the microrod (Figure 4c), demonstrating its efficient waveguide character. As shown in Figure 4d,e, Cy3 is attached at the left end of the microtubes (Cy3-tube-e, top) and microrods (Cy3-rod-e, bottom) with the excitation laser positioned at the right end of the tube to examine the sensing capability of both features. The optical loss coefficient analysis is carried out in Figure 4f as in Figure 2f, demonstrating the optical loss coefficient of Cy3-tube-e to be 0.117 μm^{-1}, approximately three times lower than that of the microrod (0.301 μm^{-1}). This demonstrates the potential of rapidly grown hexagonal Alq_3 tubular microstructures for applications such as remote bio/chemical sensors due to its advanced capabilities of remote sensing via efficient PL of the sensing molecules attached to the tube.

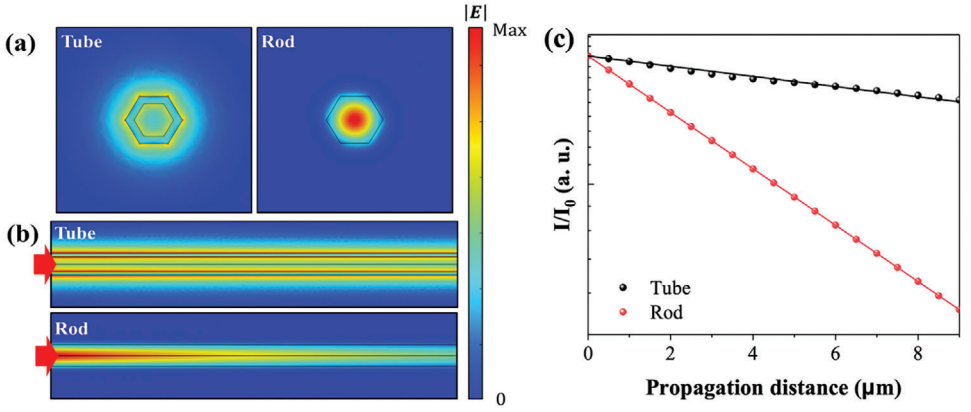

Figure 3. a) Eigenmodes of the Alq_3 microtube (left) and microrod (right) in the radial direction around the source (260 nm far from the source). b) E-field propagation (amplitude of E-field) along the longitudinal axes of the Alq_3 microtube (Tube) and microrod (Rod) with 520 nm light excited from the left end (the red arrows). c) Normalized intensities of the Alq_3 microtube (Tube) and microrod (Rod) as functions of propagation distance; the black and red lines represent an exponential decay fit of the plots.

3. Conclusion

We demonstrated a rapid growth of Alq_3 microtubes through the solution self-assembly method by introducing $BMIMBF_4$ ionic liquid. The high electron affinity of $BMIMBF_4$ ionic liquid accelerates the aggregation of the Alq_3 molecules expediting the growth of Alq_3 microstructures. Moreover, $BMIMBF_4$ ions lead to a weathering process that etches out the Alq_3 molecules from the core of the microrods, creating Alq_3 microtubes within a few minutes. The fabricated Alq_3 microtube shows a strong PL emission with outstanding waveguide characteristics with a low optical loss coefficient of 0.054 μm^{-1}. Moreover, a significantly enhanced FRET effect by the guided PL in Cy3-attached Alq_3 microtube, with a low optical loss coefficient of 0.117 μm^{-1}, is also demonstrated as an application to remote bio/chemical sensing. We believe this rapid synthesis of the 1D microstructures using organic semiconductors can be effectively utilized to develop an advanced optical components in microscale.

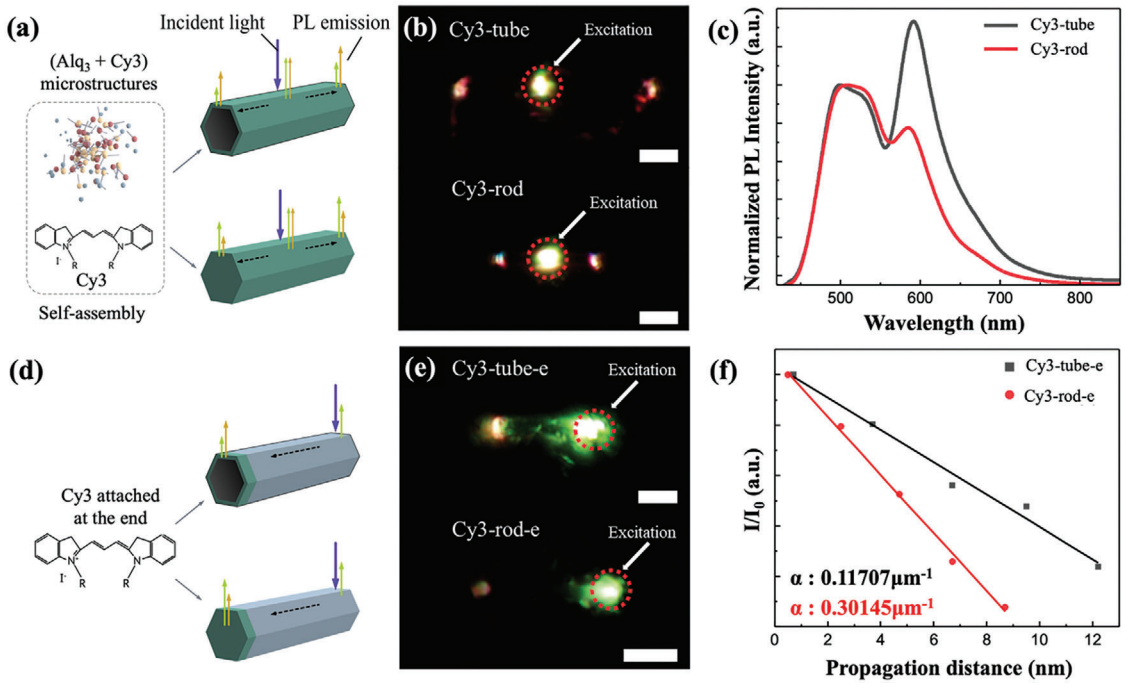

Figure 4. a) Schematic illustration of Cy3-tube and Cy3-rod fabricated by adding Cy3 during self-assembly process b) CCD images of Cy3-attached Alq_3 microtube (top) and microrod (bottom) with excitation laser positioned at the center and the corresponding c) PL spectra of Cy3-tube and Cy3-rod. d) Schematic illustration of Cy3-tube-e and Cy3-rod-e fabricated by drop-casting of Cy3 at the end of the microstructures e) CCD images of Alq_3 microtube (top) and microrod (bottom) with Cy3 attached only at the left ends of the samples. f) Logarithmic plots of the relative peak intensities at 590 nm of the Cy3-attached samples, as functions of propagation distance; the black and red lines represent an exponential decay fit of the samples. (scale bar: 5 μm).

4. Experimental Section

Materials and Instruments: Alq_3, $BMIMBF_4$, and Cy3 were purchased from Sigma–Aldrich. SEM images of the Alq_3 microstructures were obtained using a field-emission SEM (TESCAN, CLARA LMH) at an accelerating voltage of 15 kV. The FL images of the Alq_3 microstructures were taken by a color CCD (AVT Marlin F-033C, $\lambda_{ex} = 435$ nm) and a microscope CLSM (Carl Zeiss, LSM700).

Fabrication of Microrods and Microtubes: Alq_3 microtubes were fabricated through a solution self-assembly procedure. Commercial Alq_3 powder was dissolved in THF with a mass concentration of 3 mg mL^{-1}. The solution (2 mL) was injected into a 1 vol.% $BMIMBF_4$ solution (10 mL) under vigorous stirring at 800 rpm. After 10 s, 1 min, 3 min, 5 min and 2 h, the solution was dropcasted on a cover glass wafer and dried in Air for 1 h at 70 °C. Cy3-attached Alq_3 microstructures were fabricated by adding Cy3 fluorescent dye during the Alq_3 solution self-assembly or by drop-casting Cy3 at one end of each sample. For characterization, the samples were prepared by selecting isolated microstructures from the randomly dispersed samples.

Waveguide Characteristic: To measure the optical waveguide characteristics, the LCM (local confocal microscope) system was modified by separating the positions of the incident laser and the detector. The incident laser source was precisely positioned with a piezoelectric positioning system (Albatross, Nanofocus Inc.) at five invervals away from the detector with each intervals being ≈2 µm. The excitation wavelength of 405 nm was used for both luminescent color CCD images and the PL spectra and was recorded with GF-033C-IRF (Allied Vision) and SR-303I-B (Andor), respectively. The intensity of the incident laser was set to 6 µW to minimize the photo-bleaching effect.

Simulations: FEM (COMSOL Multiphysics 6.1) was used to calculate the eigenmodes and propagation characteristics of the Alq_3 microtube and microrod. The refractive index $n = 1.74 + 0.0061i$ at 520 nm for Alq_3 was obtained from the ellipsometry in the previous report.[28] The dimension of the Alq_3 microstructures was determined based on the average size of the Alq_3 microstructures in the SEM images. The width and length for both microtube and microrods were set as 325 nm and infinity, respectively. The thickness of the microtube wall is set to 86.6 nm. The substrate is excluded to reduce the effect of substrate and to confirm the loss effect caused only by waveguiding. The light is incident one port with waveguide mode. The intensity along position is calculated by integrating the intensity of light at the cross section at each point and normalized by incident point.

Supporting Information

Supporting Information is available from the Wiley Online Library or from the author.

Acknowledgements

D.Kim and J.Kim contributed equally to this work. This work was supported by the National Research Foundation of Korea (NRF) grant funded by the Korea Government Ministry of Science and ICT (MSIT) (NRF2021R1A4A5031805), and U.S. Air Force Office of Scientific Research (AFOSR) Young Investigator Program (YIP) (Grant No. FA9550-23-1-0159).

Conflict of Interest

The authors declare no conflict of interest.

Data Availability Statement

The data that support the findings of this study are available from the corresponding author upon reasonable request.

Keywords

Alq_3, hexagonal microtubes, ionic liquid, optical waveguide, solution self-assembly

Received: December 3, 2023
Revised: February 24, 2024
Published online:

[1] a) J. Broeng, D. Mogilevstev, S. E. Barkou, A. Bjarklev, *Opt. Fiber Technol.* **1999**, *5*, 305; b) H. Ma, A. K. Y. Jen, L. R. Dalton, *Adv. Mater.* **2002**, *14*, 1339; c) L. Tong, R. R. Gattass, J. B. Ashcom, S. He, J. Lou, M. Shen, I. Maxwell, E. Mazur, *Nature* **2003**, *426*, 816; d) S. Chen, M.-P. Zhuo, X.-D. Wang, G.-Q. Wei, L.-S. Liao, *PhotoniX* **2021**, *2*, 2.

[2] a) S. Lal, S. Link, N. J. Halas, *Nat. Photonics* **2007**, *1*, 641; b) Y. S. Zhao, H. Fu, A. Peng, Y. Ma, D. Xiao, J. Yao, *Adv. Mater.* **2008**, *20*, 2859; c) R. Yan, D. Gargas, P. Yang, *Nat. Photonics* **2009**, *3*, 569; d) J. Clark, G. Lanzani, *Nat. Photonics* **2010**, *4*, 438; e) D. Tian, Y. Chen, *Adv. Opt. Mater.* **2021**, *9*, 2002264.

[3] a) K. Takazawa, J.-i. Inoue, K. Mitsuishi, T. Takamasu, *Phys. Rev. Lett.* **2010**, *105*, 067401; b) Y. Yan, Y. S. Zhao, *Adv. Funct. Mater.* **2012**, *22*, 1330. c) E. H. Cho, B.-G. Kim, S. Jun, J. Lee, D. H. Park, K.-S. Lee, J. Kim, J. Kim, J. Joo, *Adv. Funct. Mater.* **2014**, *24*, 3684;

[4] a) C. R. Martin, L. S. Van Dyke, Z. Cai, W. Liang, *J. Am. Chem. Soc.* **1990**, *112*, 8976; b) M. Steinhart, J. H. Wendorff, A. Greiner, R. B. Wehrspohn, K. Nielsch, J. Schilling, J. Choi, U. Gösele, *Science* **2002**, *296*, 1997. c) J.-K. Lee, W.-K. Koh, W.-S. Chae, Y.-R. Kim, *Chem. Commun.* **2002**, 138; d) L. Zhao, W. Yang, Y. Ma, J. Yao, Y. Li, H. Liu, *Chem. Commun.* **2003**, 2442; e) D. O'Carroll, I. Lieberwirth, G. Redmond, *Nat. Nanotechnol.* **2007**, *2*, 180.

[5] a) H. Liu, Y. Li, S. Xiao, H. Gan, T. Jiu, H. Li, L. Jiang, D. Zhu, D. Yu, B. Xiang, Y. Chen, *J. Am. Chem. Soc.* **2003**, *125*, 10794; b) Q. Tang, H. Li, Y. Liu, W. Hu, *J. Am. Chem. Soc.* **2006**, *128*, 14634; c) Q. Liao, H. Fu, J. Yao, *Adv. Mater.* **2009**, *21*, 4153; d) Y. S. Zhao, J. Wu, J. Huang, *J. Am. Chem. Soc.* **2009**, *131*, 3158; e) R. Li, H. Li, Y. Song, Q. Tang, Y. Liu, W. Xu, W. Hu, D. Zhu, *Adv. Mater.* **2009**, *21*, 1605.

[6] Y. S. Zhao, H. B. Fu, F. Q. Hu, A. D. Peng, W. S. Yang, J. N. Yao, *Adv. Mater.* **2008**, *20*, 79.

[7] a) H. R. Darrell, C. Iksoo, *Nanotechnology* **1996**, *7*, 216; b) A. Greiner, J. H. Wendorff, *Angew. Chem., Int. Ed.* **2007**, *46*, 5670; c) H. Cho, S.-Y. Min, T.-W. Lee, *Macromol. Mater. Eng.* **2013**, *298*, 475.

[8] S. M. Yoon, J. Lee, J. H. Je, H. C. Choi, M. Yoon, *ACS Nano* **2011**, *5*, 2923.

[9] a) A. L. Briseno, S. C. B. Mannsfeld, C. Reese, J. M. Hancock, Y. Xiong, S. A. Jenekhe, Z. Bao, Y. Xia, *Nano Lett.* **2007**, *7*, 2847; b) P. Hui, R. Chandrasekar, *Adv. Mater.* **2013**, *25*, 2963; c) Q. Li, Y. Jia, L. Dai, Y. Yang, J. Li, *ACS Nano* **2015**, *9*, 2689.

[10] a) L. Zang, Y. Che, J. S. Moore, *Acc. Chem. Res.* **2008**, *41*, 1596; b) C. Zhang, Y. Yan, Y. S. Zhao, J. Yao, *Acc. Chem. Res.* **2014**, *47*, 3448.

[11] a) Y. S. Zhao, A. Peng, H. Fu, Y. Ma, J. Yao, *Adv. Mater.* **2008**, *20*, 1661; b) J.-J. Wu, H. Gao, X.-D. Wang, Y. Wu, L. Jiang, L.-S. Liao, *Adv. Opt. Mater.* **2023**, *11*, 2200815.

[12] E. Cho, J. Choi, S. Jo, D.-H. Park, Y. K. Hong, D. Kim, T. S. Lee, *ChemPlusChem* **2019**, *84*, 1130.

[13] a) A. Facchetti, *Chem. Mater.* **2011**, *23*, 733; b) H. Yao, J. Hou, *Angew. Chem., Int. Ed.* **2022**, *61*, e202209021.

[14] S. Kim, C. Cui, J. Huang, H. Noh, D. H. Park, D. J. Ahn, *Adv. Mater.* **2020**, *32*, 2005238.

[15] a) Y. S. Zhao, J. Xu, A. Peng, H. Fu, Y. Ma, L. Jiang, J. Yao, *Angew. Chem., Int. Ed.* **2008**, *47*, 7301; b) W. Hu, Y. Chen, H. Jiang, J. Li, G. Zou, Q. Zhang, D. Zhang, P. Wang, H. Ming, *Adv. Mater.* **2014**, *26*, 3136.

[16] a) N. Chandrasekhar, M. A. Mohiddon, R. Chandrasekar, *Adv. Opt. Mater.* **2013**, *1*, 305; b) U. Venkataramudu, D. Venkatakrishnarao, N. Chandrasekhar, M. A. Mohiddon, R. Chandrasekar, *Phys. Chem. Chem. Phys.* **2016**, *18*, 15528.
[17] a) G. John, M. Masuda, Y. Okada, K. Yase, T. Shimizu, *Adv. Mater.* **2001**, *13*, 715; b) Z. Wang, C. J. Medforth, J. A. Shelnutt, *J. Am. Chem. Soc.* **2004**, *126*, 15954; c) Y. S. Zhao, W. Yang, D. Xiao, X. Sheng, X. Yang, Z. Shuai, Y. Luo, J. Yao, *Chem. Mater.* **2005**, *17*, 6430.
[18] P. A. Gaikwad, P. Samadder, S. Som, D. Chopra, P. P. Neelakandan, A. Srivastava, *Nanoscale* **2023**, *15*, 14380.
[19] a) M. J. Muldoon, C. M. Gordon, I. R. Dunkin, *J. Chem. Soc., Perkin Trans. 2* **2001**, 433; b) J. L. Anderson, J. Ding, T. Welton, D. W. Armstrong, *J. Am. Chem. Soc.* **2002**, *124*, 14247; c) Z. He, P. Alexandridis, *Phys. Chem. Chem. Phys.* **2015**, *17*, 18238.
[20] a) M. M. Hoffmann, M. P. Heitz, J. B. Carr, J. D. Tubbs, *J. Dispersion Sci. Technol.* **2003**, *24*, 155; b) Y. He, Z. Li, P. Simone, T. P. Lodge, *J. Am. Chem. Soc.* **2006**, *128*, 2745; c) Z. Lei, B. Chen, Y. M. Koo, D. R. MacFarlane, *Chem. Rev.* **2017**, *117*, 6633; d) G. L. Sternhagen, S. Gupta, Y. Zhang, V. John, G. J. Schneider, D. Zhang, *J. Am. Chem. Soc.* **2018**, *140*, 4100.
[21] a) J. G. Huddleston, H. D. Willauer, R. P. Swatloski, A. E. Visser, R. D. Rogers, *Chem. Commun.* **1998**, 1765; b) J. D. Holbrey, K. R. Seddon, *Clean Products and Processes* **1999**, *1*, 223; c) S. K. Singh, A. W. Savoy, *J. Mol. Liq.* **2020**, *297*, 112038; d) G. Kaur, H. Kumar, M. Singla, *J. Mol. Liq.* **2022**, *351*, 118556.
[22] a) G. Zhao, Z. Schwartz, M. Wieland, F. Rupp, J. Geis-Gerstorfer, D. L. Cochran, B. D. Boyan, *J. Biomed. Mater. Res., Part A* **2005**, *74A*, 49; b) M.-P. Zhuo, Y.-C. Tao, X.-D. Wang, S. Chen, L.-S. Liao, *J. Mater. Chem. C* **2018**, *6*, 9594.
[23] H. Bi, H. Zhang, Y. Zhang, H. Gao, Z. Su, Y. Wang, *Adv. Mater.* **2010**, *22*, 1631.
[24] T. Fukushima, H. Kaji, *Org. Electron.* **2012**, *13*, 2985.
[25] J.-S. Hu, H.-X. Ji, A.-M. Cao, Z.-X. Huang, Y. Zhang, L.-J. Wan, A.-D. Xia, D.-P. Yu, X.-M. Meng, S.-T. Lee, *Chem. Commun.* **2007**, 3083.
[26] C. Cheng, J. Li, X. Cheng, *J. Lumin.* **2017**, *188*, 252.
[27] W. Sun, S. Guo, C. Hu, J. Fan, X. Peng, *Chem. Rev.* **2016**, *116*, 7768.
[28] Y. J. Cho, H. J. Kim, W. O. N. Chegal, H. M. Cho, U. B. Baek, S. H. Nahm, J.-I. Lee, H. Y. Chu, *Int. J. Mod. Phys. B* **2006**, *20*, 4353.